

3. LOSS-REGION BOUNDARIES

Having studied the drift orbit properties in Chapter 2, the determination of the loss region boundaries is next.

3.1 Grazing Orbit

First to be considered are orbits initiating at $(x_i, z_i) \leftrightarrow (r_i, \theta_i)$ and intersecting the wall at a position $(x_w, z_w) \leftrightarrow (r_w, \theta_w)$. Evaluating P_ϕ for this initial condition and substituting into (2.6) yields a quadratic in $\cos\chi$ which has the solution:

$$\cos\chi = \chi_{wi} \left[1 - \sqrt{(R_w/R_i)(1-\chi_{wi}^{-2})} \right] \quad (3.1)$$

$$\text{where } \chi_{wi} = \frac{Ze}{mv} \left(\frac{\psi_w - \psi_i}{x_w - x_i} \right),$$

$$\text{and } \psi_w \equiv \psi(r_w), \psi_i \equiv \psi(r_i).$$

Real solutions require $|\chi_{wi}| \geq 1$ and $|\cos\chi| \leq 1$. Orbits grazingly incident on a circular wall, in the tokamak mid-plane are easily determined from (3.1). More generally, (3.1) can be used to obtain orbits incident on the wall out of the mid-plane by numerically finding a local minimum (maximum) in $\cos\chi$ versus poloidal angle, θ' , of the wall-orbit intersection for the upper (lower) loss boundary. For example, in TFTR, there is a class of guiding center orbits (0.15 - to 1-MeV α for $a = 85$ cm, $I = 2.5$ MA) which intersect the wall three times. The corresponding $\cos\chi$ vs θ' plot is shown in Fig. 3.1;

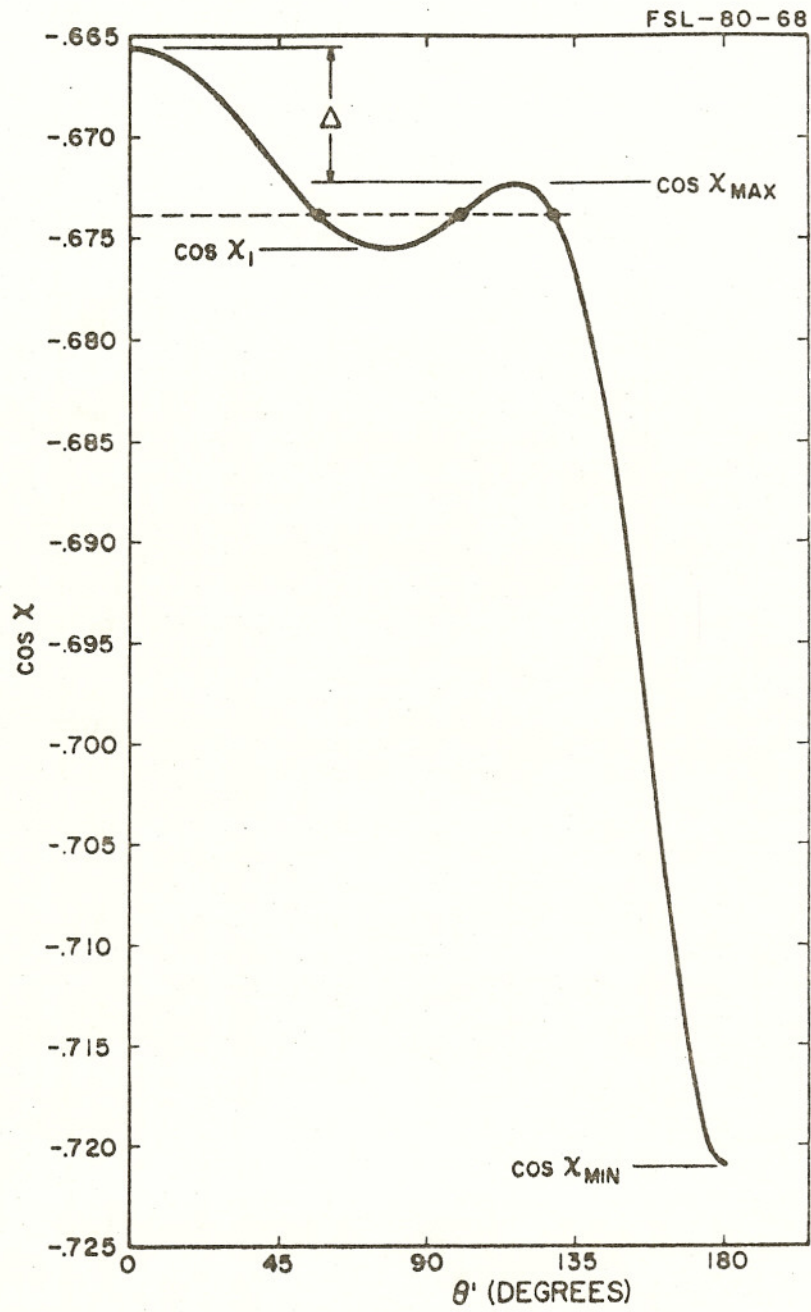


Figure 3.1 Plot of $\cos \chi$ versus poloidal angle, θ' , of wall-orbit intersections for a 1-MeV α in TFTR ($I = 2.5$ MA, $a = 85$ cm), having a birth position on the x-axis at $x_1 = 72$ cm.

note that for $\cos\chi_1 < \cos\chi < \cos\chi_{\max}$, there are three θ' -values for one value of $\cos\chi$, corresponding to three wall-orbit intersections. However, the differential loss fraction, f_ρ , for the interval Δ , is negligible ($f_\rho = \Delta/2 \leq .5\%$) so the loss boundaries are the maximum (minimum) in $\cos\chi$ as shown in Figure 3.1.

While the solution to (3.1) may satisfy the above mathematical conditions, it may also correspond to a disconnected branch of the orbit hitting the wall (see Fig. 3.2). It is necessary to test for this condition by moving along the orbit, from its birth point to the wall-orbit intersection position. For a valid intersection, the solution to (2.6) must be real for every r -value in the range, $r_i \leq r \leq r_w$. If a disconnected region does exist, i.e. no real solution to (2.6), then the grazing orbit solution must be rejected.

3.2 Stagnation Orbit

If the solution for a grazing orbit fails any of the above tests, the next loss boundary to consider is a stagnation orbit. At the unstable stagnation point $(x_s, 0)$, the orbit is characterized [18] by $dz/dx = 0$, or equivalently $dh/dr = \kappa/R_0$, where $\kappa = \text{sgn}(x_s)$. By evaluating P_ϕ at the unstable stagnation point (pitch angle = χ_s) and substituting into (2.6), a quadratic in $\cos\chi_s$ is obtained which has the solution:

$$\cos\chi_s = V_s \left(1 - \sqrt{1 - V_s^{-2}} \right), \quad V_s = \frac{Z\kappa\psi'_s}{mv}, \quad (3.2)$$

where $\psi'_s \equiv d\psi/dr$ at $r = |x_s|$. A second equation for $\cos\chi_s$ is obtained

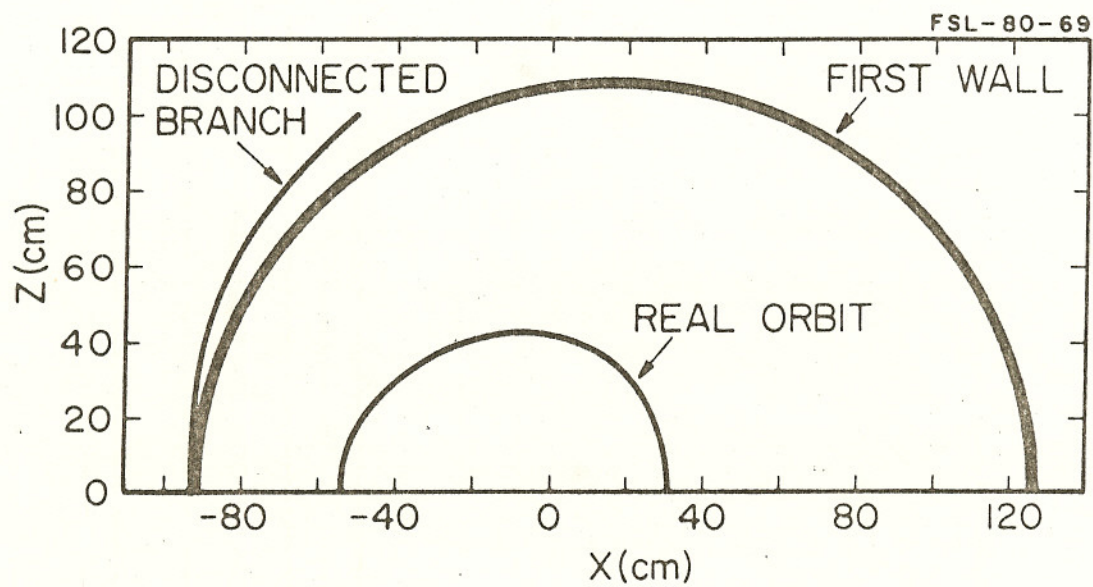


Figure 3.2 An example of a disconnected guiding-center orbit which grazingly intersects the TFTR wall.

from (3.1) for a particle initiating at $(x_s, 0) \leftrightarrow (r_s, \text{Arccos}(\text{sgn}(x_s)))$ with pitch angle, χ_s , and moving to $(x_i, z_i) \leftrightarrow (r_i, \theta_i)$; equating the result to (3.2) gives:

$$x_{si} \left[1 - \sqrt{(R_i/R_s)(1-x_{si}^{-2})} \right] - v_s \left(1 - \sqrt{1-v_s^{-2}} \right) \equiv G(x_s) = 0 \quad (3.3)$$

This last equation must be solved numerically for $r_s = |x_s|$, given the initial position. From symmetry, the pitch angle at initiation is:

$$\cos \chi = x_{si} \left[1 - \sqrt{(R_s/R_i)(1-x_{si}^{-2})} \right]. \quad (3.4)$$

Real solutions to (3.3) and (3.4) require $|x_{si}| \geq 1$, $|\cos \chi_s| \leq 1$ and $|v_s| \geq 1$.

A special case occurs when the stagnation orbit solutions are desired for an initial point $(x_i, 0)$ lying outside $x_c^- < x < x_c^+$. The corresponding pitch angle is obtained from (3.2) in the limit as

$x_s \rightarrow x_i$:

$$\cos \chi = v_i \left(1 - \sqrt{1-v_i^{-2}} \right), \quad v_i = \frac{Zek\psi_i!}{mv} \quad (3.5)$$

As before $|v_i| \geq 1$ for real solutions to (3.5). More generally (3.5) determines the pitch angle for any orbit which is a point on the x-axis; for example, in Fig. 2.2b, the transition from $\chi = 70$ to $\chi = 90$ corresponds to a "point" orbit with $\chi = 80.51^\circ$. For birth points on the x-axis, with $x_i < x_c^-$ or $x_i > x_c^+$, the "fattest" banana (last trapped orbit) corresponds to a stagnation orbit, for which $x_s = x_i$, with a pitch angle determined by (3.5). A particle born at

$(x_c^\pm, 0)$ gyrates about that point until a perturbation (due to finite gyroradius effects or collisions) causes the particle to leave the x-axis, along a guiding-center path determined by (2.6). The values of x_c^\pm are found by solving $dG/dx = 0$ at $x_s = x_i$, from (3.3); typical values of x_c^\pm for TFTR are listed in Table 3.1. A useful property of these critical positions, x_c^\pm , is that the unstable stagnation point, x_s , occurs outside the interval $x_c^- \leq x \leq x_c^+$; this realization speeds the numerical search for x_s in (3.3). As with the grazing orbits, it is necessary to move along a stagnation orbit, beginning at the birth point, to assure that the path intersects the wall.

Table 3.1: Values of x_c^\pm in TFTR I

Particle	$x_c^-(\text{cm})$	$x_c^+(\text{cm})$
3.52 MeV α	-20.7	109.5
3.7 MeV α	-21.1	106.1
1.0 MeV α	-13.4	>127
14.7 MeV p	-33.8	51.2
3.0 MeV p	-19.6	121.0

3.3 Orbits with $\chi = 0$ (180°)

The final loss boundary to consider is $\cos\chi = \text{sgn}(x_i)$, i.e. $\chi = 0$ (180°), even if a valid stagnation orbit-wall intersection occurs. As before, the orbit must be traced from the birth point to the wall to verify intersection. If only a stagnation orbit-wall intersection exists, this is the appropriate loss boundary; likewise, if only a valid $\chi = 0$ (180°) intersection occurs. If both are valid intersections,

the latter is the correct loss boundary. Examples of these last two cases are shown in Fig. 3.3 for a 0.82-MeV He^3 in TFTR ($I=1\text{MA}$, $a=85\text{ cm}$).

3.4 Summary of Boundaries

Table 3.2 summarizes the various loss boundaries and the associated equations, used in calculating the loss region in velocity space. By solving an analytical form for the guiding-center drift-orbit equation, it is possible to find the pitch angle, χ , corresponding to an orbit (defined as type A) which has an arbitrary birth position and intersects the wall at any point. This includes a general form for χ , corresponding to x-type stagnation orbits (type B orbits), occurring for both $R < R_0$ and $R > R_0$. Study of the drift orbits [4,22] also shows that particles born near the inner (outer) plasma edge can have a minimum (maximum) loss orbit (type C orbit), for $\chi = 0$ (180°).

Table 3.2: Summary of Loss Boundaries

Type		Equation(s)	Figure(s) for Examples
A	Grazing	3.1	2.2
B	Stagnation	3.2-3.4	2.2-4
	Point	3.5	-
C	$\chi = 0, 180^\circ$	-	2.3a,3c

These orbit types are used to define the boundaries of the velocity-space loss-region for fp's escaping to the wall from any given birth point. If a type A orbit exists and is continuously connected between

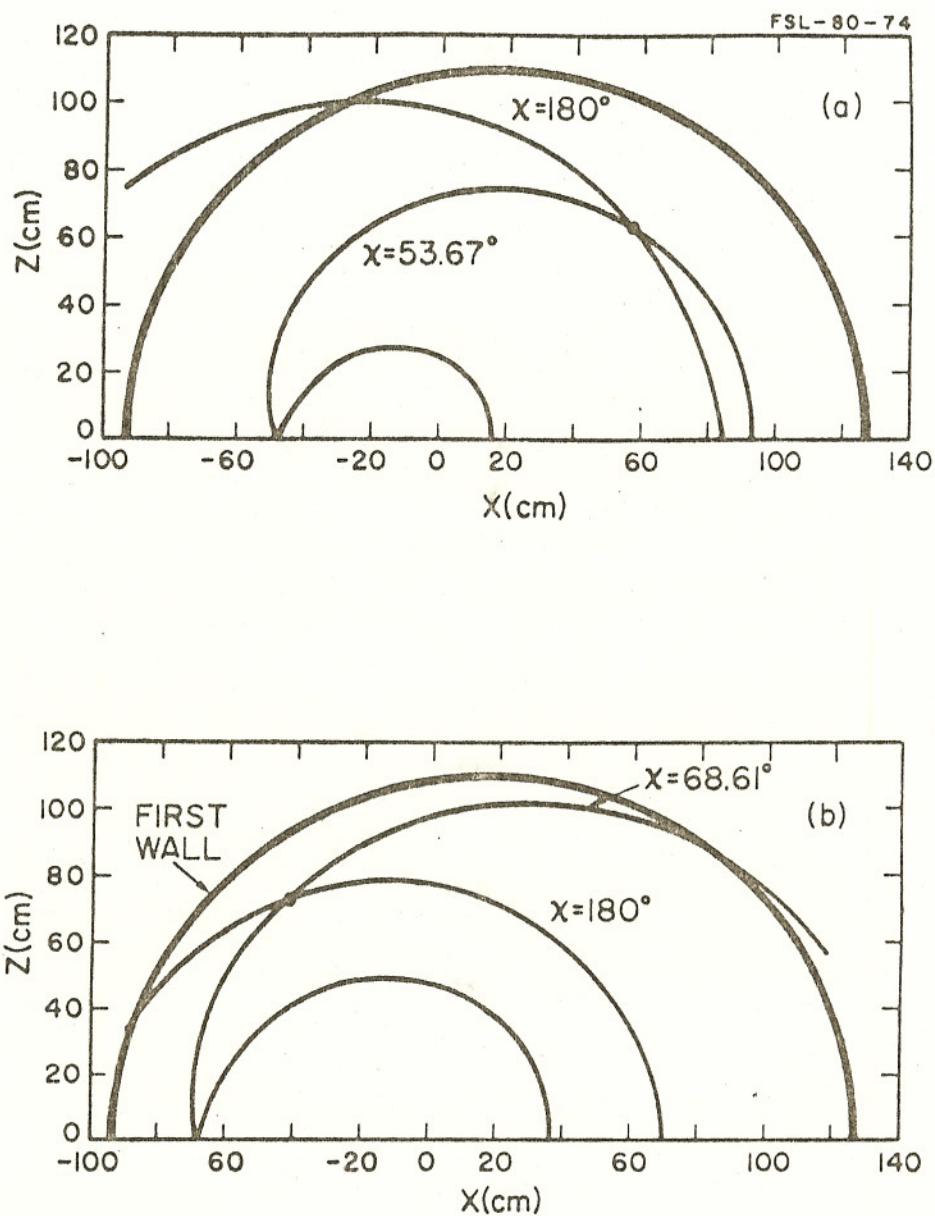


Figure 3.3 Stagnation and $\chi=180^\circ$ guiding center orbits for a 0.82-MeV He^3 in TFTR ($I=1\text{MA}$, $a=85\text{ cm}$). Fig. 3.3a shows an example of only the $\chi=180^\circ$ orbit intersecting the wall for a birth point at (57 cm, 63.17 cm). Fig. 3.3b shows an example of both the stagnation and $\chi=180^\circ$ orbits hitting the wall from an initial point of (-42.5 cm, 73.61 cm).

the birth point and wall, it is the appropriate loss boundary to the outboard (inboard) edge of the wall. If not, B, and then C, are successively examined. If both B and C satisfy these criteria, then orbit C is the appropriate loss boundary. When these conditions for particle loss are combined, the loss region in velocity space is obtained. An example for alpha losses from the TFTR I plasma is shown in Fig. 3.4 for a parabolic current density profile. It is noteworthy that losses occur across the entire plasma but only for energies above 350 keV. Fig. 3.4 differs from the plots of Rome et al. [18], because in the present calculations the wall is removed from the plasma edge. The intersection of the loss region with the $v_{||}$ axis occurs for $\cos\chi = \pm 1$, which implies $|x_{wi}| = 1$, from (3.1). The resulting velocity is:

$$v_{\max} = \frac{Ze}{mR_0} \left| \frac{\psi_w - \psi_i}{h_w - h_i} \right| \quad (3.6)$$

where $h_w = (R_0 + x_w)/R_0$ and x_w corresponds to the inner and outer edges of the first wall; similarly, h_i corresponds to the initial point.

Using these results in the next chapter, the wall loading from each birth point is calculated for all wall segments between the wall-orbit intersections, corresponding to the loss boundaries, $x_{\min} \leq x \leq x_{\max}$. If all these boundaries fail to exist, there is no loss region for the given birth point, i.e., the fp is totally contained.

For later reference it is convenient to define the zero loss region (ZLR); all orbits originating inside the ZLR are completely confined and cannot reach the wall. The ZLR can occur in two ways

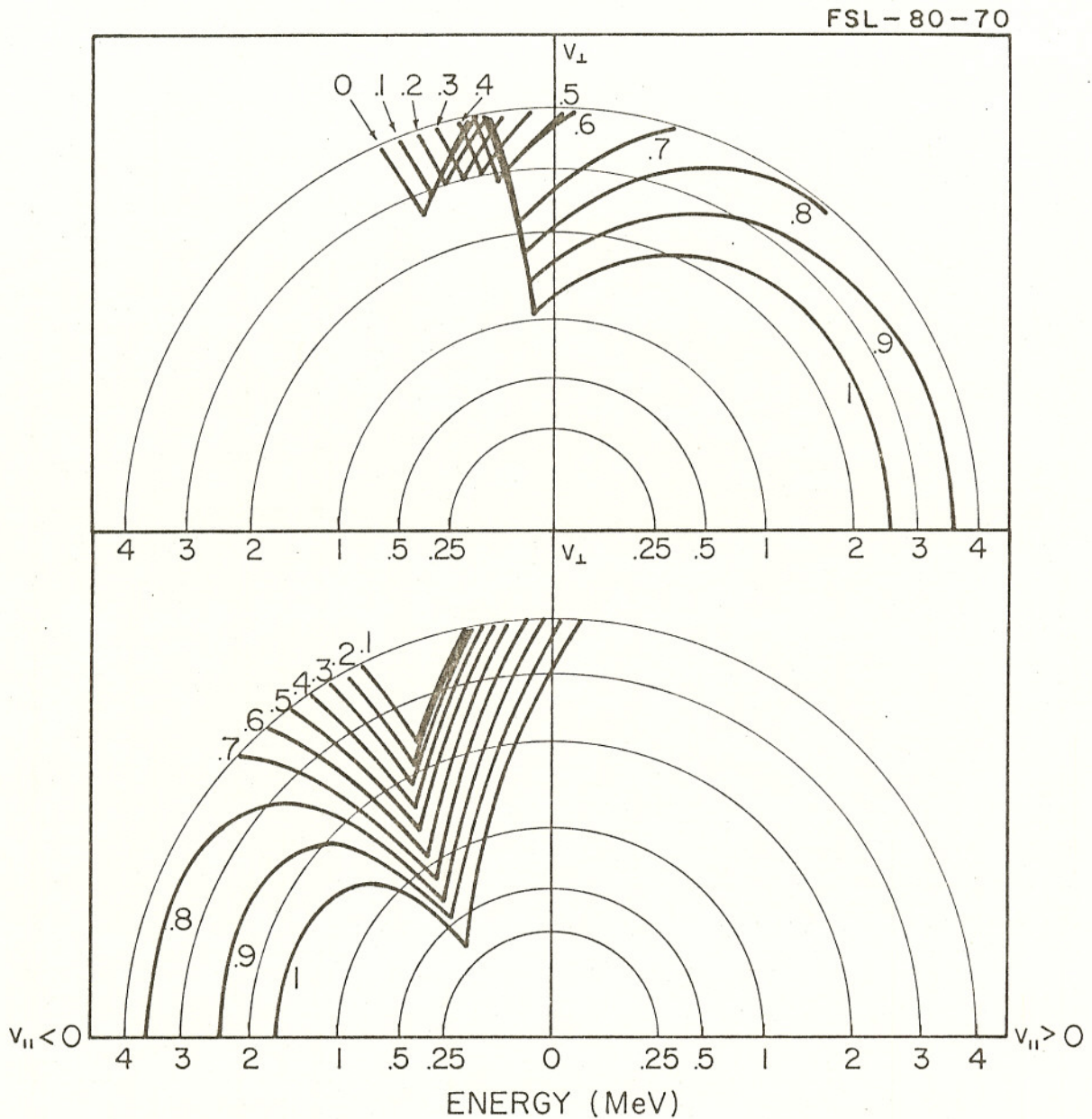


Figure 3.4 Loss region in $v_{||}$ - v_{\perp} space for an α incident on the first wall from birth points on the x-axis in the TFTR-I plasma. The assumed form for current density is $J = J_0[1-(r/a)^2]$. Numbers of each curve in the upper graph indicate birth points (for $R < R_0$) as the ratio $(-x_i/a)$; on the lower figure the numbers indicate birth points (for $R > R_0$) as $(+x_i/a)$.

(see Fig. 3.5): either being bounded by the inner loop of an unstable stagnation orbit which barely intersects the outboard edge of the wall, or being bounded by the second loop of a double stagnation orbit [4]. In the extreme case, the loss fraction, F_{ℓ} , becomes zero as the ZLR covers the whole plasma for a sufficiently large plasma-wall separation.

FSL-78-42 R

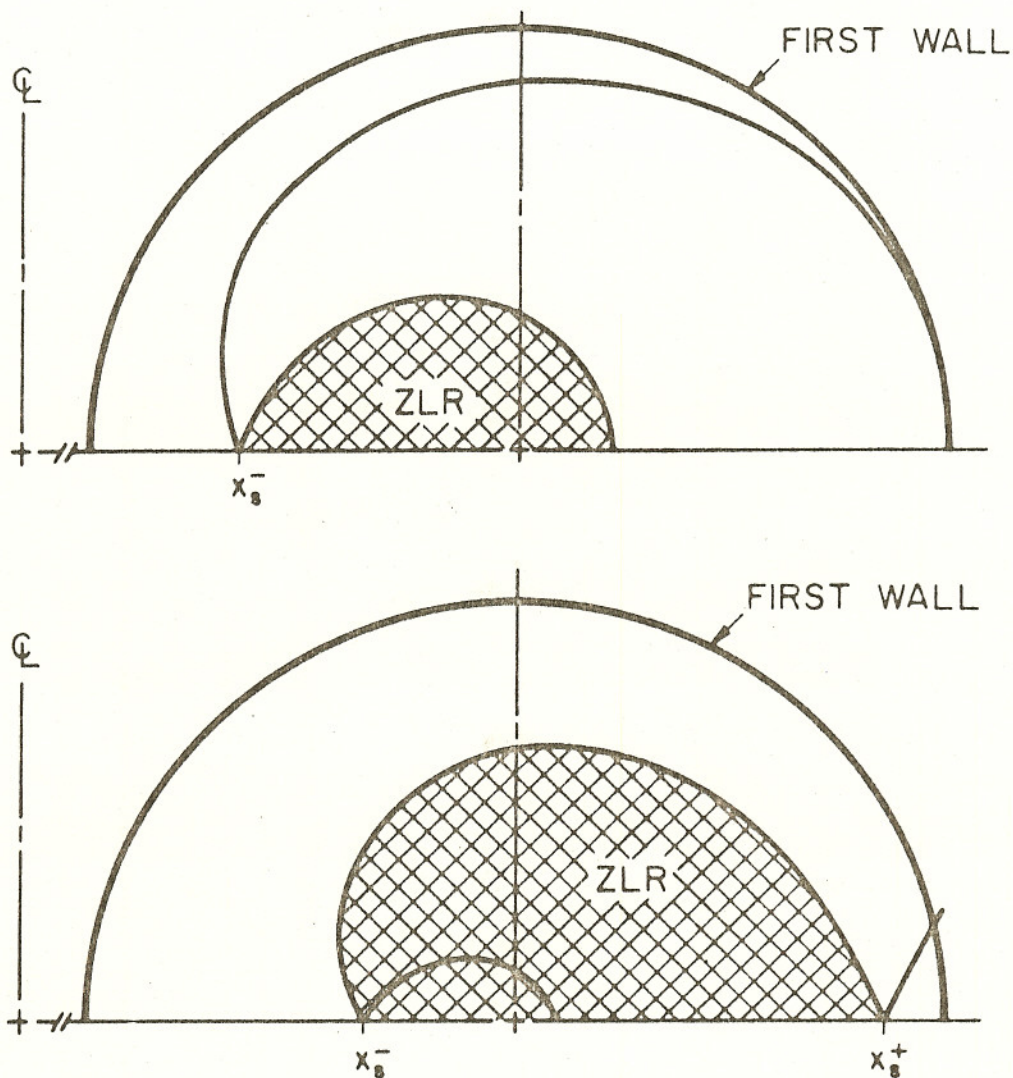


Figure 3.5 In the top figure the zero loss region is bounded by the inner loop of the stagnation orbit which grazingly intersects the outboard edge of the first wall; orbits originating inside the ZLR cannot reach the wall. In the bottom figure, the zero loss region is bounded by the second loop of a double stagnation orbit.